Edgar I. Ergueta
Mem. ASME
Department of Mechanical Engineering,
University of California,
Berkeley, CA 94720
e-mail: edgar.ergueta@wdc.com

Robert Seifried
Professor
Institute of Engineering and Computational Mechanics,
University of Stuttgart,
70550 Stuttgart, Germany
e-mail: seifried@itm.uni-stuttgart.de

Roberto Horowitz
James Fife Endowed Chair
Department of Mechanical Engineering,
University of California,
Berkeley, CA 94720
e-mail: horowitz@me.berkeley.edu

A Robust Approach to Dynamic Feedback Linearization for a Steerable Nips Mechanism

This paper presents two different control strategies for paper position control in printing devices. The first strategy is based on standard feedback linearization plus dynamic extension (dynamic feedback linearization). Even though this controller is very simple to design, we show that it is not able to handle actuator multiplicative uncertainties, and therefore, it fails when it is implemented on the experimental setup. The second strategy we present uses similar concepts, but it is more robust since feedback linearization is used only to linearize the kinematics of the system and internal loops are used to locally control the actuator's positions and velocities. In this paper, not only do we formally prove the robustness of the second control strategy but we also show its successful implementation. [DOI: 10.1115/1.4003261]

1 Introduction

Static feedback linearization is a nonlinear technique widely used for the control of Multiple-Input-Multiple-Output (MIMO) nonlinear systems. As explained in Refs. [1,2], it consists in differentiating each of the outputs several times until at least one of the inputs appears. At that point we obtain a decoupling matrix, which needs to be inverted in order to linearize the system. Once the system is linearized through this transformation, pole placement is used to achieve the desired control objective. Unfortunately, sometimes this decoupling matrix is singular, making static feedback linearization fail.

A common solution to this problem, usually referred to as dynamic feedback linearization, has been presented in Refs. [1–4]. Such a solution consists on adding integrators to some of the input channels in order to delay the appearance of the inputs when differentiating the outputs. Proceeding in this way, it might be possible to construct a new nonsingular decoupling matrix. However, even if we succeed in finding an invertible decoupling matrix, the control strategy can be very sensible to model parameter uncertainties. For such cases, it is sometimes advised to modify this standard technique in order to gain robustness.

In particular, in this paper we show how a *Dynamic Feedback Linearization* controller cannot be directly implemented in a mechatronic application for paper position control on printing devices, and a *Robust Feedback Linearization Plus Inner Loops* controller needs to be used instead. This controller has been presented in Refs. [5,6]; it uses feedback linearization to linearize only the kinematics of the system and uses internal loops to locally control the actuators' positions and velocities.

The mechatronic application discussed in this paper has been presented in Refs. [7–10]. The idea behind this mechanism is shown in Fig. 1 [11], and it consists on two steerable nips that permit the control of the longitudinal, lateral, and angular positions of a sheet while it is being driven forward. As mentioned in Refs. [7,8], this mechanism resembles that of a two-wheel robot [12]; however, not only does the two-wheel robot have one less degree of freedom than the steerable nips system but also the control law proposed by Ref. [12] fails to account for singularities that arise when the steering angle of the wheels approaches zero. Moreover, whereas the two-wheel robot requires three inputs to follow a reference trajectory, the steerable nips require four in order to steer and rotate each roller (see Fig. 1).

The asymptotic stability of the *Robust Feedback Linearization Plus Inner Loops* control strategy has been already proved in Refs. [5,6]. Such stability analysis was conducted primarily to tune the control system gains in order to achieve a set of performance parameters, mainly to reduce tracking errors by a prespecified amount in a finite specified time. However, we will now show its robustness to actuator multiplicative uncertainties by analyzing its convergence as time goes to infinity and by seeking to attain exponential stability of the nominal system. Furthermore, we will contrast its robustness to that of the *Dynamic Feedback Linearization* controller.

The remainder of this paper is organized as follows: Section 2 describes the steerable nips mechanism and presents its model. Section 3 presents the development of the *Dynamic Feedback Linearization* controller designed for this application, and Sec. 4 presents the *Robust Feedback Linearization Plus Inner Loops* controller, which has been successfully implemented on the experimental setup. Section 5 compares the robustness of both control strategies, and Sec. 6 presents experimental results. Finally, some concluding remarks are stated in Sec. 7.

2 Steerable Nips Mechanism

As mentioned in Sec. 1, the idea behind the steerable nips mechanism is shown in Fig. 1. Specifically, this figure shows a sheet moving along a flat surface through the steerable nips mechanism and in the direction of the arrow labeled $\underline{v}$. This mechanism has been designed so that it can correct lateral sheet position errors without having to translate any actuators and without inflicting any damage on the paper. This is possible by steering the two rollers shown in the figure, which are underneath a backer ball. As a result, each roller is in contact with the sheet at only one point, letting the sheets safely move laterally while they are being driven forward. The roller is driven by a servo motor (*process direction motor*) attached to a rotating table, which is in turn steered by another servo motor (*steering motor*). A complete description of this mechanism can be found in Refs. [8–10]. Note

Contributed by the Dynamic Systems Division of ASME for publication in the JOURNAL OF DYNAMIC SYSTEMS, MEASUREMENT, AND CONTROL. Manuscript received March 19, 2009; final manuscript received October 26, 2010; published online February 22, 2011. Assoc. Editor: Won-jong Kim.

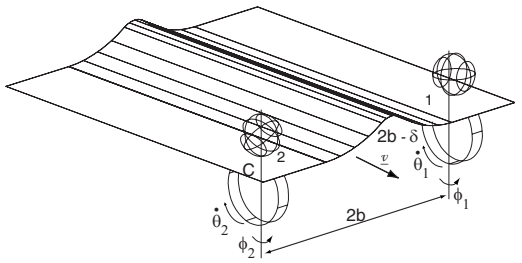

Fig. 1 Steerable nips with paper buckle

that in Fig. 1, the two rollers, located at points 1 and 2, are separated by a fixed distance $2b$.

In Refs. [5,6], we were able to show asymptotic convergence of the robust feedback linearization plus inner loops control strategy (described in Sec. 4) only for a sheet of finite length and thus for finite time. Such constraints were necessary because one of the control objectives was that the sheet's leading edge needed to track a desired reference, which moved at a constant speed. In practice, however, sheets have finite length and, therefore, the leading edge of the sheet only needs to be controlled until it reaches the beginning of the image transfer station (ITS) of the printing device. By maintaining this control architecture, as time goes to infinity, so does the length of the page, and the control effort to control the position of the leading edge of the sheet becomes increasingly larger. Thus, in order to conduct a robustness analysis, we will require the sheet track a constant longitudinal speed in the longitudinal direction instead of requiring the position of the leading edge of the paper track a reference position trajectory moving with a constant speed. As will be shown in Sec. 5.1, by imposing velocity rather than position control, in the longitudinal direction, the tracking errors in the nominal system converge exponentially rather than just asymptotically since we no longer require to control the position of the leading edge of a sheet whose length goes to infinity.

Furthermore, in Refs. [5,6] we used the leading right corner of the sheet (point C in Fig. 1) as a reference for controlling the lateral and longitudinal positions of the page. However, since we will consider a page of infinite length, we would like to completely decouple lateral from longitudinal positions as in Fig. 2. Specifically, we will refer to the lateral position of the page x as the point along the lateral edge of the sheet that is in contact with the lateral sensor shown in this figure. Similarly, we will define the longitudinal position of the sheet y as the point along the leading edge of the sheet that is in contact with the longitudinal sensor located along the process direction in the middle of rollers 1 and 2; ϕ will represent the angular position of the sheet. Note that since the two rollers steer independently, the sheet can also

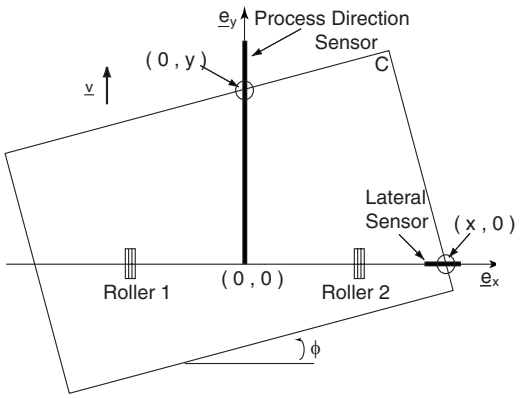

Fig. 2 Top view of steerable nips

buckle or stretch. Thus, we need to keep buckling at a minimum and make sure that the sheet never stretches. As shown in Fig. 1, we define the amount of buckling of the sheet δ as the difference between the distance separating points 1 and 2 as measured along the paper $(2b-\delta)$ and along a straight line $(2b)$. Furthermore, $\dot{\theta}_i$ $(i=1,2)$ represents the angular velocity of the rollers in the direction parallel to the sheet, and ϕ_i $(i=1,2)$ represents their angular position in the direction perpendicular to the sheet.

The steerable nips mechanism has four nonholonomic constraints, which come from nonslip conditions on the rollers and local velocities (of the paper) being zero in the direction perpendicular to the rotation of the rollers at the point of contact with the rollers. Thus, its kinematics model is derived so that these constraints are satisfied at all times; such a model is derived in Refs. [9,10], and it is represented by the following equations:

$$\dot{x} = r_2\dot{\theta}_2\left(\sin\phi_2 - \frac{x+b}{2b}\tan\phi\cos\phi_2\right) + r_1\dot{\theta}_1\frac{x-b}{2b}\tan\phi\cos\phi_1 := f_x(\underline{x})$$

$$\dot{y} = -r_2\dot{\theta}_2\left(\sin\phi_2\tan\phi + \frac{y\tan\phi+b}{2b}\cos\phi_2\right) + r_1\dot{\theta}_1\frac{y\tan\phi-b}{2b}\cos\phi_1 := f_y(\underline{x})$$

$$\dot{\phi} = \frac{1}{2b}(r_1\cos\phi_1\dot{\theta}_1 - r_2\cos\phi_2\dot{\theta}_2) := f_\phi(\underline{x})$$

$$\dot{\delta} = r_2\sin\phi_2\dot{\theta}_2 - r_1\sin\phi_1\dot{\theta}_1 := f_\delta(\underline{x}) \tag{1}$$

where r_1 and r_2 are the radii of the two rollers, and the state vector is given by $\underline{x}=[x\ \ \phi\ \ \delta\ \ \phi_1\ \ \phi_2\ \ \dot{\theta}_2\ \ \dot{\theta}_2\ \ \dot{\phi}_1\ \ \dot{\phi}_2]^T$. It should be noted that y is not a state because, as mentioned earlier, we are controlling the longitudinal velocity of the page at the location of the ITS $(y=L)$ instead of its longitudinal position. As mentioned in Ref. [8], a simple model that adequately describes both the process direction and steering actuator dynamics is given by

$$\ddot{\theta}_i + \alpha_{pi}\dot{\theta}_i = \beta_{pi}V_{pi} \quad (i=1,2)$$

$$\ddot{\phi}_i + \alpha_{si}\dot{\phi}_i = \beta_{si}V_{si} \quad (i=1,2) \tag{2}$$

where V_{ji} is the input voltage to each motor, and α_{ji} and β_{ji} are coefficients that depend on the inertias and rotational viscous damping coefficients of the different components of the steerable nips mechanism. Subindexes p and s stand for process direction and steering actuators, respectively. Using Eqs. (1) and (2) we obtain the following state space representation:

$$\frac{d}{dt}\begin{bmatrix} x \\ \phi \\ \delta \\ \phi_1 \\ \phi_2 \\ \dot{\theta}_1 \\ \dot{\theta}_2 \\ \dot{\phi}_1 \\ \dot{\phi}_2 \end{bmatrix} = \begin{bmatrix} f_x(\underline{x}) \\ f_\phi(\underline{x}) \\ f_\delta(\underline{x}) \\ \dot{\phi}_1 \\ \dot{\phi}_2 \\ -\alpha_{p1}\dot{\theta}_1 \\ -\alpha_{p2}\dot{\theta}_2 \\ -\alpha_{s1}\dot{\phi}_1 \\ -\alpha_{s2}\dot{\phi}_2 \end{bmatrix} + \begin{bmatrix} 0 & 0 & 0 & 0 \\ 0 & 0 & 0 & 0 \\ 0 & 0 & 0 & 0 \\ 0 & 0 & 0 & 0 \\ 0 & 0 & 0 & 0 \\ \beta_{p1} & 0 & 0 & 0 \\ 0 & \beta_{p2} & 0 & 0 \\ 0 & 0 & \beta_{s1} & 0 \\ 0 & 0 & 0 & \beta_{s2} \end{bmatrix} \begin{bmatrix} V_{p1} \\ V_{p2} \\ V_{s1} \\ V_{s2} \end{bmatrix}$$

$$\underline{y} = \begin{bmatrix} x & \dot{y}_L & \phi & \delta \end{bmatrix} \tag{3}$$

where $f_x(\underline{x})$, $f_\phi(\underline{x})$, and $f_\delta(\underline{x})$ are defined in Eq. (1), and $\dot{y}_L$ is equal to $f_y(\underline{x})$ evaluated at $y=L$.

3 Dynamic Feedback Linearization Controller

In this section, we will first show that pure feedback linearization cannot be applied to the steerable nips system. Then, we will show that even though a strategy based on dynamic feedback linearization can be designed, it cannot be implemented on the experimental setup due to actuator multiplicative uncertainties.

As mentioned in Sec. 2, the control objective is to control the lateral and angular positions of the sheet before it arrives at the ITS as well as its longitudinal velocity at that location. This needs to be accomplished within a finite prespecified time and through the use of four control inputs. Two of these inputs rotate and steer one roller, and the other two inputs rotate and steer the other roller.

If we simply use static feedback linearization for this system, differentiating outputs x, ϕ, and δ twice and output $\dot{y}_L$ once, we obtain an expression of the form

$$\begin{bmatrix} \ddot{x} & \ddot{y}_L & \ddot{\phi} & \ddot{\delta} \end{bmatrix}^T = A(\underline{x}) + B(\underline{x}) \begin{bmatrix} V_{p1} & V_{p2} & V_{s1} & V_{s2} \end{bmatrix}^T \tag{4}$$

where the decoupling matrix $B(\underline{x})$ is singular. Thus, following the work presented in Refs. [1–4], in order to obtain a new nonsingular decoupling matrix, we add an integrator to the input channels corresponding to V_{p1} and V_{p2}. Proceeding in this way, V_{p1} and V_{p2} become new states of the system and their derivatives become two of the control inputs. We then define the new states z_i $(i=1,2)$ and new control inputs w_i $(i=1-4)$ as

$$z_1 = V_{p1} \quad z_2 = V_{p2}$$

$$w_1 = \dot{z}_1 \quad w_2 = \dot{z}_2$$

$$w_3 = V_{s1} \quad w_4 = V_{s2} \tag{5}$$

and obtain the following enlarged system:

$$\frac{d}{dt}\begin{bmatrix} x \\ \phi \\ \delta \\ \phi_1 \\ \phi_2 \\ \dot{\theta}_1 \\ \dot{\theta}_2 \\ \dot{\phi}_1 \\ \dot{\phi}_2 \\ z_1 \\ z_2 \end{bmatrix} = \begin{bmatrix} f_x(\underline{x}) \\ f_\phi(\underline{x}) \\ f_\delta(\underline{x}) \\ \dot{\phi}_1 \\ \dot{\phi}_2 \\ -\alpha_{p1}\dot{\theta}_1 + \beta_{p1} z_1 \\ -\alpha_{p2}\dot{\theta}_2 + \beta_{p2} z_2 \\ -\alpha_{s1}\dot{\phi}_1 \\ -\alpha_{s2}\dot{\phi}_2 \\ 0 \\ 0 \end{bmatrix} + \begin{bmatrix} 0 & 0 & 0 & 0 \\ 0 & 0 & 0 & 0 \\ 0 & 0 & 0 & 0 \\ 0 & 0 & 0 & 0 \\ 0 & 0 & 0 & 0 \\ 0 & 0 & 0 & 0 \\ 0 & 0 & 0 & 0 \\ 0 & 0 & \beta_{s1} & 0 \\ 0 & 0 & 0 & \beta_{s2} \\ 1 & 0 & 0 & 0 \\ 0 & 1 & 0 & 0 \end{bmatrix} \begin{bmatrix} w_1 \\ w_2 \\ w_3 \\ w_4 \end{bmatrix}$$

$$\underline{y} = \begin{bmatrix} x & \dot{y}_L & \phi & \delta \end{bmatrix}^T \tag{6}$$

where we define the enlarged state vector as $\underline{x}_e = [x \ \phi \ \delta \ \phi_1 \ \phi_2 \ \dot{\theta}_2 \ \dot{\theta}_2 \ \dot{\phi}_1 \ \dot{\phi}_2 \ z_1 \ z_2]^T$. Differentiating outputs x, ϕ, and δ three times and output $\dot{y}_L$ twice, we now obtain

$$\begin{bmatrix} \dddot{x} & \dddot{y}_L & \dddot{\phi} & \dddot{\delta} \end{bmatrix}^T = A_e(\underline{x}_e) + B_e(\underline{x}_e) \begin{bmatrix} w_1 & w_2 & w_3 & w_4 \end{bmatrix}^T \tag{7}$$

where $A_e(\underline{x}_e)$ is a nonlinear vector and $B_e(\underline{x}_e)$ is a nonlinear square matrix. By computing the inverse of $B_e(\underline{x}_e)$, it can be shown that this matrix is nonsingular as long as the sheet is always moving in the process direction $(\dot{\theta}_1, \dot{\theta}_2 \neq 0)$. Thus, if we apply the feedback linearization control law

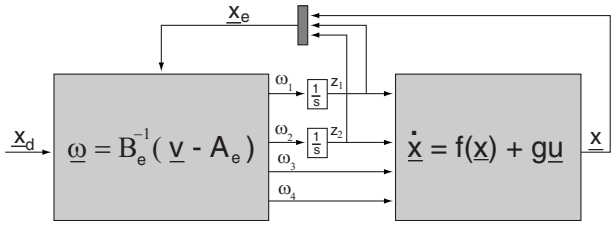

Fig. 3 ***Dynamic Feedback Linearization*** **controller**

$$\begin{bmatrix} w_1 & w_2 & w_3 & w_4 \end{bmatrix}^T = B_e(\underline{x}_e)^{-1}(\underline{v}(\underline{x}_e) - A_e(\underline{x}_e))$$

$$\underline{v}(\underline{x}_e) = \begin{bmatrix} \dddot{x}_d + k_x(\ddot{x}_d - \ddot{x}) + l_x(\dot{x}_d - \dot{x}) + \lambda_x(x_d - x) \\ \dddot{y}_d + k_y(\ddot{y}_d - \ddot{y}) + l_y(\dot{y}_d - \dot{y}) \\ \ddot{\phi}_d + k_\phi(\ddot{\phi}_d - \ddot{\phi}) + l_\phi(\dot{\phi}_d - \dot{\phi}) + \lambda_\phi(\phi_d - \phi) \\ \ddot{\delta}_d + k_\delta(\ddot{\delta}_d - \ddot{\delta}) + l_\delta(\dot{\delta}_d - \dot{\delta}) + \lambda_\delta(\delta_d - \delta) \end{bmatrix} \tag{8}$$

by proper selection of gains k's, l's, and λ's through pole placement, we can guarantee that the state errors converge to zero. Furthermore, since the enlarged system consist of 11 states and the relative degree is also 11, there are no internal dynamics, and we can conclude that the enlarged system is exponentially stable. The block diagram for this control strategy is shown in Fig. 3. Using this control law, for a sheet moving at a nominal velocity of $v=0.5$ m/s and having initial errors $(x(0), \dot{y}_L(0), \phi(0), \delta(0)) = (8 \text{ mm}, 30 \text{ mm/s}, 2.5 \text{ m rad}, 0.1 \text{ mm})$ we obtain the simulation results shown in Fig. 4.

The dashed line in Fig. 4 shows that the dynamic feedback linearization controller does a good job in reducing initial errors when we only consider a nominal plant for the actuators. However, this control strategy fails when we consider actuator multiplicative uncertainties as in Fig. 5, where P_{ji} is the actuator plant given by Eq. (2), and Δ_{ji} is the uncertainty dynamics. This is true even for relatively mild uncertainty dynamics as the one given by

$$\Delta_{pi}(s) = \frac{\delta_{pi}}{(s + m_{pi})^2} \quad \Delta_{si}(s) = \frac{\delta_{si}}{s + m_{si}} \quad i = 1,2 \tag{9}$$

In particular, the solid line in Fig. 4 shows the results when the multiplicative uncertainties in Eq. (9) are introduced to the system with $m_{pi}=m_{si}=1.5$ and $\delta_{pi}=\delta_{si}=1$ for $i=1,2$. Notice that the control strategy fails not only because it is not able to eliminate errors in the longitudinal velocity of the sheet but also because it stretches the page (negative values for the error in buckling), which should never occur. In Sec. 5, we will compare the robustness of this control strategy to the one presented in Sec. 4. In fact, we will use the small gain theorem to show that whereas the controller presented in Sec. 4 is robust to actuator multiplicative uncertainties, the same cannot be concluded for the controller just discussed in this section. Finally, note that since the process direction actuator controls velocity (as opposed to the steering actuator, which controls position), a second order model was used for its uncertainty, which greatly simplifies the analysis performed in Sec. 5. However, we would have obtained similar results even if a first order model was used as the uncertainty for the process direction actuator. In fact, we could replace the second order model in Eq. (9) by two first order models in parallel, with one of them having an arbitrarily large pole and corresponding large gain.

4 Robust Feedback Linearization Plus Inner Loops Controller

The control strategy presented in this section uses similar concepts to those described in Sec. 3. However, instead of linearizing the whole system, we use feedback linearization only to linearize the kinematics and use inner loops to locally control the actuator's

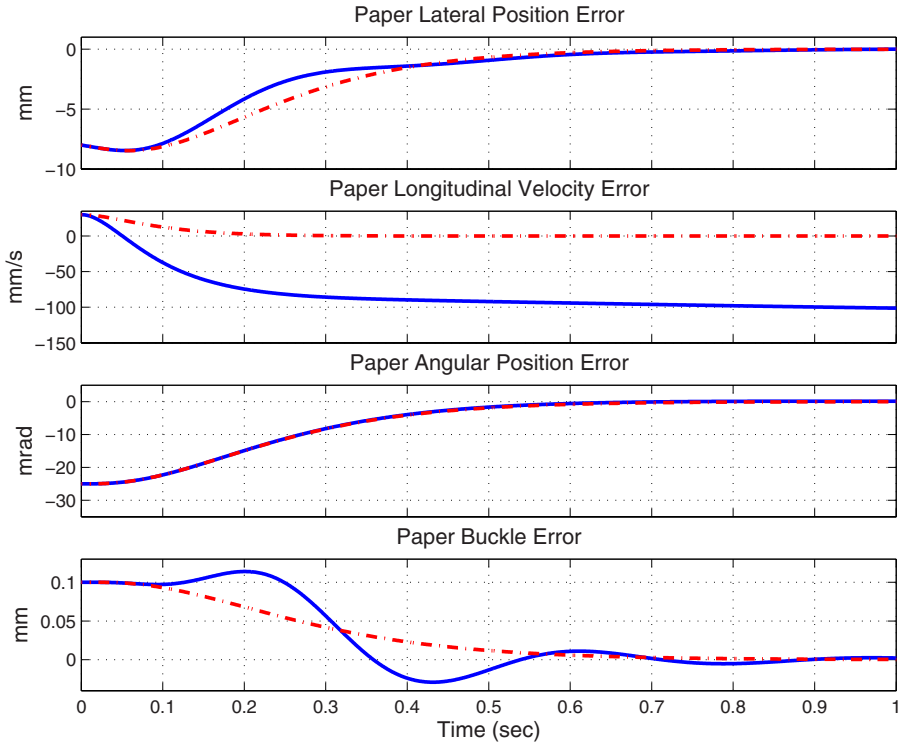

Fig. 4 Simulation results using the *Dynamic Feedback Linearization* controller. The solid and dashed lines represent the results with and without actuator multiplicative uncertainty, respectively.

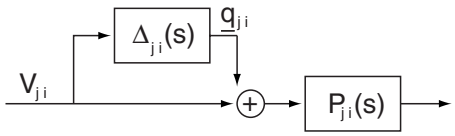

Fig. 5 Actuator multiplicative uncertainty ($j=s,p$; $i=1,2$)

rotational velocities and steering positions. Figure 6 shows the control strategy implemented to the real system. There, the feedback linearization controller C_{FBL} produces desired rotational accelerations and desired steering velocities, which after being integrated, are used as references to locally control the actuators, which are represented by blocks P_{ji} ($j=\mathrm{p,s}$; $i=1,2$). It should be

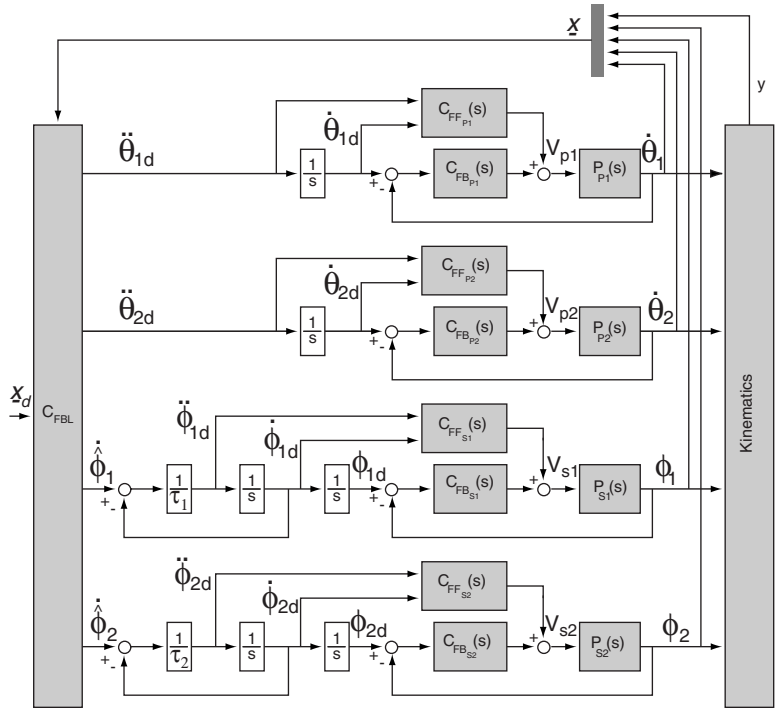

Fig. 6 *Robust Feedback Linearization Plus Inner Loops* controller

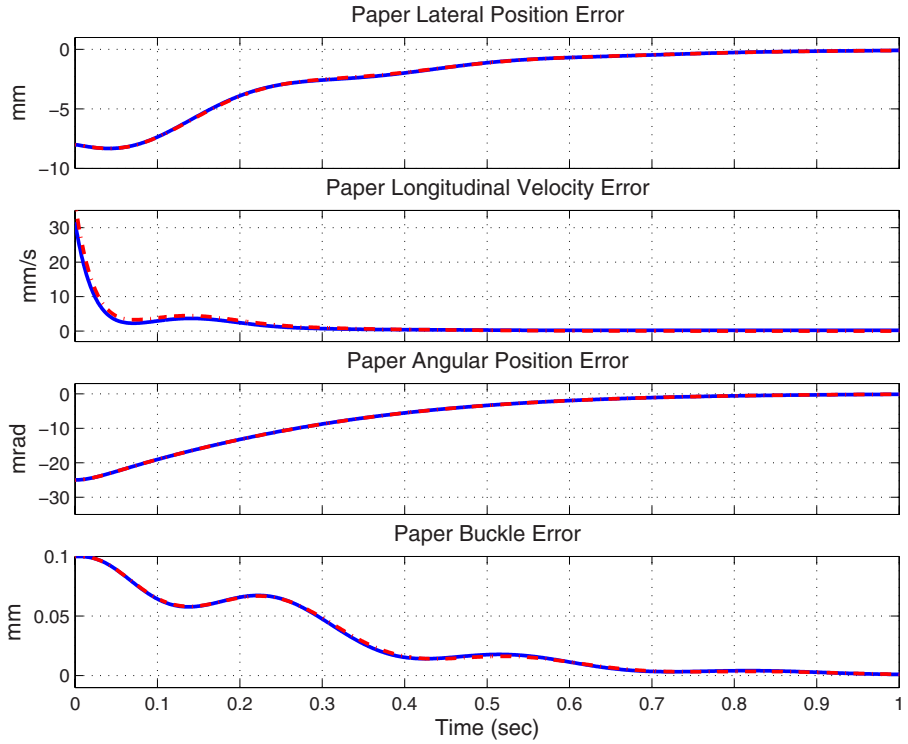

Fig. 7 Simulation results using the *Robust Feedback Linearization Plus Inner Loops* controller. Note that the results without uncertainty (dashed line) and those with uncertainty (solid line) are almost indistinguishable.

noticed that by feedback linearizing only the kinematics and not the dynamics of the system (as opposed to the controller presented in Sec. 3) the control system gains robustness since the local controllers can efficiently handle actuator uncertainties. This will be formally proven in Sec. 5. The actuators in Fig. 6 are controlled through feedback plus feedforward; these local controllers are

$$C_{\mathrm{FB}_{pi}}(s) = \eta_{pi} + \frac{\gamma_{pi}}{s} \quad C_{\mathrm{FF}_{pi}} = \frac{1}{\beta_{pi}}\left(1 + \frac{\alpha_{pi}}{s}\right)$$

$$C_{\mathrm{FB}_{si}}(s) = \eta_{si} + \gamma_{si}s \quad C_{\mathrm{FF}_{si}} = \frac{1}{\beta_{si}}\left(1 + \frac{\alpha_{si}}{s}\right) \tag{10}$$

where η's and γ's are controller gains, α's and β's are the actuator coefficients defined in Eq. (2), and subindex i corresponds to each of the two rollers. In order to be able to estimate the desired steering acceleration $\ddot{\phi}_{id}$ (needed for feedforward control), we use two first order filters, a technique called dynamic surface control described in Ref. [13]. Note that if filter gain τ_i is sufficiently small, the value of the signal generated by the controller C_{FBL} $\dot{\hat{\phi}}_i$, will be very close to that of the filter output $\dot{\phi}_{id}$. In order to obtain the feedback linearization law C_{FBL}, we first need to differentiate outputs x, ϕ, and δ twice, and output $\dot{y}_L$ once, obtaining the expression

$$\begin{bmatrix} \ddot{x} & \ddot{y}_L & \ddot{\phi} & \ddot{\delta} \end{bmatrix}^T = A_r(\underline{x}) + B_r(\underline{x})\begin{bmatrix} \ddot{\theta}_1 & \ddot{\theta}_2 & \dot{\phi}_1 & \dot{\phi}_2 \end{bmatrix}^T \tag{11}$$

where, again, $A_r(\underline{x})$ is a nonlinear vector, and $B_r(\underline{x})$ is a nonlinear square matrix. Note that by computing the inverse of $B_r(\underline{x})$, it can be shown that this matrix is invertible as long as the sheet is always moving along the process direction ($\dot{\theta}_1, \dot{\theta}_2 \neq 0$). Thus, we can safely apply the following feedback linearization law (block C_{FBL} in Fig. 6):

$$\begin{bmatrix} \ddot{\theta}_{1d} & \ddot{\theta}_{2d} & \dot{\hat{\phi}}_1 & \dot{\hat{\phi}}_2 \end{bmatrix}^T = B_r(\underline{x})^{-1}(\underline{v}(\underline{x}) - A_r(\underline{x})) \tag{12}$$

$$\underline{v}(\underline{x}) = \begin{bmatrix} \ddot{x}_d + (k_x + \lambda_x)(\dot{x}_d - \dot{x}) + k_x\lambda_x(x_d - x) \\ \ddot{y}_d + k_y(\dot{y}_d - \dot{y}_L) \\ \ddot{\phi}_d + (k_\phi + \lambda_\phi)(\dot{\phi}_d - \dot{\phi}) + k_\phi\lambda_\phi(\phi_d - \phi) \\ \ddot{\delta}_d + (k_\delta + \lambda_\delta)(\dot{\delta}_d - \dot{\delta}) + k_\delta\lambda_\delta(\delta_d - \delta) \end{bmatrix} \tag{13}$$

where k's and λ's are controller gains. Figure 7 shows simulation results for the controller just presented using the same initial conditions as those used for the control system described in Sec. 3. This figure shows results for the cases with and without the multiplicative uncertainties defined in Eq. (9). Contrary to the results obtained using the controller described in Sec. 3, the *Robust Feedback Linearization Plus Inner Loops* controller corrects the initial errors of the sheet in both cases. The exponential stability of the closed-loop system and its robustness to actuator multiplicative uncertainties will be proved in Sec. 5.

5 Robustness Analysis

In this section, we will first show the exponential stability of the *Robust Feedback Linearization Plus Inner Loops* nominal control (presented in Sec. 4) through the indirect method of Lyapunov, and then we will show its robustness to actuator multiplicative uncertainties. Finally, we will compare its robustness to that of the *Dynamic Feedback Linearization* control system presented in Sec. 3.

5.1 Stability of the Robust Feedback Linearization Plus Inner Loops Control Strategy. Let us first define paper coordinate and actuator errors by

$$\tilde{x} = x_d - x \quad \tilde{\phi} = \phi_d - \phi$$

$$\tilde{\delta} = \delta_d - \delta \quad \varepsilon_i = \dot{\hat{\phi}}_i - \dot{\phi}_{id} \quad (i = 1,2)$$

$$\varepsilon_{pi} = \dot{\theta}_{id} - \dot{\theta}_i \quad \varepsilon_{si} = \phi_{id} - \phi_i \quad (i = 1,2) \tag{14}$$

and let us also define the following surface errors:

$$s_x = \dot{\tilde{x}} + \lambda_x \tilde{x} \quad s_y = \dot{\tilde{y}} = \dot{y}_d - \dot{y}_L$$

$$s_\phi = \dot{\tilde{\phi}} + \lambda_\phi \tilde{\phi} \quad s_\delta = \dot{\tilde{\delta}} + \lambda_\phi \tilde{\delta}$$

$$s_{\varepsilon_{p1}} = \dot{\varepsilon}_{p1} + \lambda_{\varepsilon_{p1}} \varepsilon_{p1} \quad s_{\varepsilon_{s1}} = \dot{\varepsilon}_{s1} + \lambda_{\varepsilon_{s1}} \varepsilon_{s1}$$

$$s_{\varepsilon_{p2}} = \dot{\varepsilon}_{p2} + \lambda_{\varepsilon_{p2}} \varepsilon_{p2} \quad s_{\varepsilon_{s2}} = \dot{\varepsilon}_{s2} + \lambda_{\varepsilon_{s2}} \varepsilon_{s2} \tag{15}$$

Combining Eqs. (11)–(14) we obtain the closed-loop expression

$$\begin{bmatrix} \ddot{x} & \dot{y}_L & \ddot{\phi} & \ddot{\delta} \end{bmatrix}^T = \underline{v}(\underline{x}) - B_r(\underline{x}) \begin{bmatrix} \dot{\varepsilon}_{p1} & \dot{\varepsilon}_{p2} & (\dot{\varepsilon}_{s1} + \varepsilon_1) & (\dot{\varepsilon}_{s2} + \varepsilon_2) \end{bmatrix}^T \tag{16}$$

Now, we are going to write the system error dynamics in terms of paper coordinate errors ($\tilde{x}, \tilde{\phi}, \tilde{\delta}$), actuator errors ($\varepsilon_{p1}$, ε_{p2}, ε_{s1}, ε_{s2}, ε_1, and ε_2), and surface errors (s_x, s_y, s_ϕ, s_δ, $s_{\varepsilon_{p1}}$, $s_{\varepsilon_{p2}}$, $s_{\varepsilon_{s1}}$, and $s_{\varepsilon_{s2}}$). First, note that we can easily obtain expressions for $\dot{\tilde{x}}$, $\dot{\tilde{\phi}}$, $\dot{\tilde{\delta}}$, $\dot{\varepsilon}_{p1}$, $\dot{\varepsilon}_{p2}$, $\dot{\varepsilon}_{s1}$, and $\dot{\varepsilon}_{s2}$ from Eq. (15).

In order to obtain an expression for $\dot{s}_x$, we need to take the derivative of s_x in Eq. (15), express Eq. (13) in terms of paper and and surface errors, and combine it to Eq. (16), as follows:

$$\begin{aligned} \dot{s}_x &= \ddot{\tilde{x}} + \lambda_x \dot{\tilde{x}} = \ddot{x}_d - \ddot{x} + \lambda_x \dot{\tilde{x}} = -k_x s_x + b_{11}\dot{\varepsilon}_{p1} + b_{12}\dot{\varepsilon}_{p2} + b_{13}\dot{\varepsilon}_{s1} \\ &\quad + b_{14}\dot{\varepsilon}_{s2} = -k_x s_x + b_{11}(s_{\varepsilon_{p1}} - \lambda_{\varepsilon_{p1}}\varepsilon_{p1}) + b_{12}(s_{\varepsilon_{p2}} - \lambda_{\varepsilon_{p2}}\varepsilon_{p2}) \\ &\quad + b_{13}(s_{\varepsilon_{s1}} - \lambda_{\varepsilon_{s1}}\varepsilon_{s1} + \varepsilon_1) + b_{14}(s_{\varepsilon_{s2}} - \lambda_{\varepsilon_{s2}}\varepsilon_{s2} + \varepsilon_2) \end{aligned} \tag{17}$$

where b_{ij} is the (i,j)th element of matrix $B_r(\underline{x})$ in Eq. (11). We can then obtain expressions for $\dot{s}_y$, $\dot{s}_\phi$, and $\dot{s}_\delta$ in a similar fashion. If we now let controller gains γ_{pi} and η_{si} $(i=1,2)$ in Eq. (10) be equal to

$$\gamma_{pi} = \frac{(\alpha_{pi} + \beta_{pi}\eta_{pi} - \lambda_{\varepsilon_{pi}})\lambda_{\varepsilon_{pi}}}{\beta_{pi}} \quad (i = 1,2)$$

$$\eta_{si} = \frac{(\alpha_{si} + \gamma_{si}\beta_{si} - \lambda_{\varepsilon_{si}})\lambda_{\varepsilon_{si}}}{\beta_{si}} \quad (i = 1,2) \tag{18}$$

we can obtain an expression for $\dot{s}_{\varepsilon_{p1}}$ as we did for $\dot{s}_x$. In fact, if we differentiate $s_{\varepsilon_{p1}}$ in Eq. (15), and combine Eqs. (2), (10), (15), and (18), we obtain

$$\begin{aligned} \dot{s}_{\varepsilon_{p1}} &= \ddot{\varepsilon}_{p1} + \lambda_{\varepsilon_{p1}}\dot{\varepsilon}_{p1} = -(\alpha_{p1} + \beta_{p1}\eta_{p1})\dot{\varepsilon}_{p1} - \gamma_{p1}\beta_{p1}\varepsilon_{p1} + \lambda_{\varepsilon_{p1}}\dot{\varepsilon}_{p1} \\ &= -(\alpha_{p1} + \beta_{p1}\eta_{p1} - \lambda_{\varepsilon_{p1}})s_{\varepsilon_{p1}} \end{aligned} \tag{19}$$

Again, expressions for $\dot{s}_{\varepsilon_{p2}}$, $\dot{s}_{\varepsilon_{s1}}$, and $\dot{s}_{\varepsilon_{s2}}$ can be obtained in a similar fashion. Finally, $\dot{\varepsilon}_i$ $(i=1,2)$ is given by

$$\dot{\varepsilon}_i = \ddot{\hat{\phi}}_i - \ddot{\phi}_{id} = \frac{\partial \dot{\hat{\phi}}_i}{\partial \underline{\Psi}}\dot{\underline{\Psi}} + \frac{\partial \dot{\hat{\phi}}_i}{\partial t} - \frac{1}{\tau_i}\varepsilon_i \tag{20}$$

where $\underline{\Psi}$ is defined by

$$\underline{\Psi} = \begin{bmatrix} \tilde{x} & s_x & s_y & \tilde{\phi} & s_\phi & \tilde{\delta} & s_\delta \end{bmatrix}^T \tag{21}$$

Note that the partial derivatives in Eq. (20) can be written in terms of paper coordinates and actuator and surface errors (Eqs. (14) and (15)); however, due to their complexity and length, they will not be explicitly written in this paper. Furthermore, the partial derivative with respect to time is equal to zero when $\underline{e}(t)=0$ (see definition of $\underline{e}(t)$ in Eq. (24)).

In summary, the system errors dynamics can then be expressed as

$$\dot{\tilde{x}} = -\lambda_x \tilde{x} + s_x$$

$$\dot{\tilde{\phi}} = -\lambda_\phi \tilde{\phi} + s_\phi$$

$$\dot{\tilde{\delta}} = -\lambda_\delta \tilde{\delta} + s_\delta$$

$$\dot{\varepsilon}_{p1} = -\lambda_{p1}\varepsilon_{p1} + s_{\varepsilon_{p1}}$$

$$\dot{\varepsilon}_{p2} = -\lambda_{p2}\varepsilon_{p2} + s_{\varepsilon_{p2}}$$

$$\dot{\varepsilon}_{s1} = -\lambda_{s1}\varepsilon_{s1} + s_{\varepsilon_{s1}}$$

$$\dot{\varepsilon}_{s2} = -\lambda_{s2}\varepsilon_{s2} + s_{\varepsilon_{s2}}$$

$$\begin{aligned} \dot{s}_x &= -k_x s_x + b_{11}(s_{\varepsilon_{p1}} - \lambda_{\varepsilon_{p1}}\varepsilon_{p1}) + b_{12}(s_{\varepsilon_{p2}} - \lambda_{\varepsilon_{p2}}\varepsilon_{p2}) \\ &\quad + b_{13}(s_{\varepsilon_{s1}} - \lambda_{\varepsilon_{s1}}\varepsilon_{s1} + \varepsilon_1) + b_{14}(s_{\varepsilon_{s2}} - \lambda_{\varepsilon_{s2}}\varepsilon_{s2} + \varepsilon_2) \end{aligned}$$

$$\begin{aligned} \dot{s}_y &= -k_y s_y + b_{21}(s_{\varepsilon_{p1}} - \lambda_{\varepsilon_{p1}}\varepsilon_{p1}) + b_{22}(s_{\varepsilon_{p2}} - \lambda_{\varepsilon_{p2}}\varepsilon_{p2}) \\ &\quad + b_{23}(s_{\varepsilon_{s1}} - \lambda_{\varepsilon_{s1}}\varepsilon_{s1} + \varepsilon_1) + b_{24}(s_{\varepsilon_{s2}} - \lambda_{\varepsilon_{s2}}\varepsilon_{s2} + \varepsilon_2) \end{aligned}$$

$$\begin{aligned} \dot{s}_\phi &= -k_\phi s_\phi + b_{31}(s_{\varepsilon_{p1}} - \lambda_{\varepsilon_{p1}}\varepsilon_{p1}) + b_{32}(s_{\varepsilon_{p2}} - \lambda_{\varepsilon_{p2}}\varepsilon_{p2}) \\ &\quad + b_{33}(s_{\varepsilon_{s1}} - \lambda_{\varepsilon_{s1}}\varepsilon_{s1} + \varepsilon_1) + b_{34}(s_{\varepsilon_{s2}} - \lambda_{\varepsilon_{s2}}\varepsilon_{s2} + \varepsilon_2) \end{aligned}$$

$$\begin{aligned} \dot{s}_\delta &= -k_\delta s_\delta + b_{41}(s_{\varepsilon_{p1}} - \lambda_{\varepsilon_{p1}}\varepsilon_{p1}) + b_{42}(s_{\varepsilon_{p2}} - \lambda_{\varepsilon_{p2}}\varepsilon_{p2}) \\ &\quad + b_{43}(s_{\varepsilon_{s1}} - \lambda_{\varepsilon_{s1}}\varepsilon_{s1} + \varepsilon_1) + b_{44}(s_{\varepsilon_{s2}} - \lambda_{\varepsilon_{s2}}\varepsilon_{s2} + \varepsilon_2) \end{aligned}$$

$$\dot{s}_{\varepsilon_{p1}} = -(\alpha_{p1} + \beta_{p1}\eta_{p1} - \lambda_{\varepsilon_{p1}})s_{\varepsilon_{p1}}$$

$$\dot{s}_{\varepsilon_{p2}} = -(\alpha_{p2} + \beta_{p2}\eta_{p2} - \lambda_{\varepsilon_{p2}})s_{\varepsilon_{p2}}$$

$$\dot{s}_{\varepsilon_{s1}} = -(\alpha_{s1} + \beta_{s1}\gamma_{s1} - \lambda_{\varepsilon_{s1}})s_{\varepsilon_{s1}}$$

$$\dot{s}_{\varepsilon_{s2}} = -(\alpha_{s2} + \beta_{s2}\gamma_{s2} - \lambda_{\varepsilon_{s2}})s_{\varepsilon_{s2}}$$

$$\dot{\varepsilon}_1 = -\frac{1}{\tau_1}\varepsilon_1 + \frac{\partial \dot{\hat{\phi}}_1}{\partial \underline{\Psi}}\dot{\underline{\Psi}} + \frac{\partial \dot{\hat{\phi}}_1}{\partial t}$$

$$\dot{\varepsilon}_2 = -\frac{1}{\tau_2}\varepsilon_2 + \frac{\partial \dot{\hat{\phi}}_2}{\partial \underline{\Psi}}\dot{\underline{\Psi}} + \frac{\partial \dot{\hat{\phi}}_2}{\partial t} \tag{22}$$

where b_{ij} is the (i,j)th element of matrix $B_r(\underline{x})$ in Eq. (11), and $\underline{\Psi}$ is defined by Eq. (21).

For simplicity, Eq. (22) can be rewritten in compact form as

$$\dot{\underline{e}}(t) = f(\underline{e}(t)) \tag{23}$$

where the error vector $\underline{e}(t)$ is given by

$$\underline{e}(t) = \begin{bmatrix} \bar{x} & \bar{y} & \bar{\phi} & \bar{\delta} & \bar{\varepsilon}_{p1} & \bar{\varepsilon}_{p2} & \bar{\varepsilon}_{s1} & \bar{\varepsilon}_{s2} & \bar{\varepsilon} \end{bmatrix}^T \tag{24}$$

and the elements of $\underline{e}(t)$ are

$$\bar{x} = \begin{bmatrix} \tilde{x} \\ s_x \end{bmatrix} \quad \bar{y} = s_y \quad \bar{\phi} = \begin{bmatrix} \tilde{\phi} \\ s_\phi \end{bmatrix}$$

$$\bar{\delta} = \begin{bmatrix} \tilde{\delta} \\ s_\delta \end{bmatrix} \quad \bar{\varepsilon}_{p1} = \begin{bmatrix} \varepsilon_{p1} \\ s_{\varepsilon_{p1}} \end{bmatrix} \quad \bar{\varepsilon}_{p2} = \begin{bmatrix} \varepsilon_{p2} \\ s_{\varepsilon_{p2}} \end{bmatrix}$$

$$\bar{\varepsilon}_{s1} = \begin{bmatrix} \varepsilon_{s1} \\ s_{\varepsilon_{s1}} \end{bmatrix} \quad \bar{\varepsilon}_{s2} = \begin{bmatrix} \varepsilon_{s2} \\ s_{\varepsilon_{s2}} \end{bmatrix} \quad \bar{\varepsilon} = \begin{bmatrix} \varepsilon_1 \\ \varepsilon_2 \end{bmatrix} \tag{25}$$

If we now define the desired trajectory by $(x_d, \phi_d, \delta_d, \dot{x}_d, \dot{y}_d, \dot{\phi}_d, \dot{\delta}_d) = (0,0,0,0,\nu,0,0)$, where ν is the nominal longitudinal velocity of the sheet, and we linearize the system

described in Eq. (22) around $\tilde{x}=\tilde{\phi}=\tilde{\delta}=\varepsilon_{p1}=\varepsilon_{p2}=\varepsilon_{s1}=\varepsilon_{s2}=s_x=s_y=s_\phi=s_\delta=s_{\varepsilon_{p1}}=s_{\varepsilon_{p2}}=s_{\varepsilon_{s1}}=s_{\varepsilon_{s2}}=\varepsilon_1=\varepsilon_2=0$, we can obtain an expression of the form

$$\dot{\underline{e}}(t) = G\underline{e}(t) \tag{26}$$

where G is given by

$$G = \begin{bmatrix} A_x & 0 & 0 & 0 & 0 & 0 & 0 & B_x^{\varepsilon_{s2}} & B_x^{\varepsilon} \\ 0 & A_y & 0 & 0 & B_y^{\varepsilon_{p1}} & B_y^{\varepsilon_{p2}} & 0 & 0 & 0 \\ 0 & 0 & A_\phi & 0 & B_\phi^{\varepsilon_{p1}} & B_\phi^{\varepsilon_{p2}} & 0 & 0 & 0 \\ 0 & 0 & 0 & A_\delta & 0 & 0 & B_\delta^{\varepsilon_{s1}} & B_\delta^{\varepsilon_{s2}} & B_\delta^{\varepsilon} \\ 0 & 0 & 0 & 0 & A_{\varepsilon_{p1}} & 0 & 0 & 0 & 0 \\ 0 & 0 & 0 & 0 & 0 & A_{\varepsilon_{p2}} & 0 & 0 & 0 \\ 0 & 0 & 0 & 0 & 0 & 0 & A_{\varepsilon_{s1}} & 0 & 0 \\ 0 & 0 & 0 & 0 & 0 & 0 & 0 & A_{\varepsilon_{s2}} & 0 \\ B_\varepsilon^x & 0 & B_\varepsilon^\phi & B_\varepsilon^\delta & B_\varepsilon^{\varepsilon_{p1}} & B_\varepsilon^{\varepsilon_{p2}} & B_\varepsilon^{\varepsilon_{s1}} & B_\varepsilon^{\varepsilon_{s2}} & A_\varepsilon \end{bmatrix} \tag{27}$$

where matrices A's depend only on controller gains, and matrices B's depend on controller gains as well as on system parameters. If we now define n_1 and n_2 as

$$n_1 = \begin{bmatrix} \bar{\varepsilon}_{p1} & \bar{\varepsilon}_{p2} & \bar{\varepsilon}_{s1} & \bar{\varepsilon}_{s2} \end{bmatrix}^T$$

$$n_2 = \begin{bmatrix} \bar{x} & \bar{y} & \bar{\phi} & \bar{\delta} & \bar{\varepsilon} \end{bmatrix}^T \tag{28}$$

we can express Eqs. (26) and (27) as

$$\begin{bmatrix} \dot{n}_1 \\ \dot{n}_2 \end{bmatrix} = \begin{bmatrix} A_{n_1} & 0 \\ B_{n_2}^{n_1} & A_{n_2} \end{bmatrix} \begin{bmatrix} n_1 \\ n_2 \end{bmatrix} \tag{29}$$

where the solutions for $n_1(t)$ and $n_2(t)$ are given by

$$n_1(t) = e^{A_{n_1}t} n_1(0)$$

$$n_2(t) = e^{A_{n_2}t} n_2(0) + \left[\int_0^t e^{A_{n_2}(t-\tau)} B_{n_2}^{n_1} e^{A_{n_1}\tau} d\tau \right] n_1(0) \tag{30}$$

It is easy to show now that by proper selection of the controller gains (λ's and k's in Eq. (13) and η's and γ's in Eq. (10)), there exist positive constants $\bar{k}$ and $\bar{\gamma}$ such that

$$\|\underline{e}(t)\| \le \bar{k}\|\underline{e}(0)\| \exp(-\bar{\gamma}t) \tag{31}$$

And, therefore, the linearized error dynamics in Eq. (26) are exponentially stable. Note that Ref. [5] details the procedure used to obtain controller gains λ's, k's, η's, and γ's. Moreover, if we define the Lyapunov function

$$v(\underline{e}) = \underline{e}^T P \underline{e} \tag{32}$$

where P is the positive definite solution to the Lyapunov equation

$$G^T P + PG = -Q \tag{33}$$

and Q is any positive definite matrix, we obtain the bounds

$$\lambda_{\min}(P)\|\underline{e}\|^2 \le v(\underline{e}) \le \lambda_{\max}(P)\|\underline{e}\|^2 \tag{34}$$

$$\dot{v}(\underline{e}) \le -\lambda_{\min}(Q)\|\underline{e}\|^2 \tag{35}$$

$$\left\| \frac{\partial v}{\partial \underline{e}} \right\| \le \lambda_{\max}(P)\|\underline{e}\| \tag{36}$$

Furthermore, it can be shown that if we rewrite Eq. (23) as

$$\dot{\underline{e}} = G\underline{e}(t) + f_1(\underline{e}(t)) \tag{37}$$

where G is given by Eq. (27), and define the Lyapunov function as in Eq. (32), where P is given by Eq. (33), then $v(\underline{e})$ satisfies inequalities (34) and (36). Moreover, since $f_1(\underline{e})$ satisfies

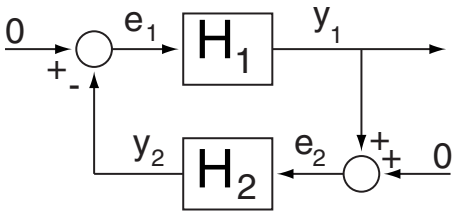

Fig. 8 Feedback connection for small gain theorem

$\lim_{\|\underline{e}\|\to 0} \frac{\|f_1(\underline{e})\|}{\|\underline{e}\|} = 0$, then for any $k>0$, $\exists r>0$ such that $\|f_1(\underline{e})\| \le k\|\underline{e}\| \forall \|\underline{e}\| < r$. In particular, if we let $k=\alpha\lambda_{\min}(Q)/2\lambda_{\max}(P)$ with $0<\alpha<1$, then $\exists r>0$ such that, for all $\|\underline{e}\|<r$, we have

$$\dot{v}(\underline{e}) \le -\lambda_{\min}(Q)(1-\alpha)\|\underline{e}\|^2 \quad \text{with} \quad 0<\alpha<1 \tag{38}$$

and thus the nonlinear system in Eq. (23) is also locally exponentially stable.

5.2 Robustness of the Robust Feedback Linearization Plus Inner Loops Control Strategy. Let us now analyze the robustness of the robust feedback linearization plus inner loops control strategy presented in Sec. 4 to actuator multiplicative uncertainties. Specifically, when we consider the actuator uncertainties given by Eq. (9) and shown in Fig. 5, the closed-loop system is given by

$$\dot{\underline{e}} = m(\underline{e},\underline{q}) = f(\underline{e}(t)) - D\underline{q}(t) = G\underline{e}(t) + f_1(\underline{e}(t)) - D\underline{q}(t) \tag{39}$$

where $f(\underline{e})$ is defined by Eq. (23), G and $f_1(\underline{e}(t))$ by Eq. (37), the error state vector $\underline{e}(t)$ is given by Eq. (24), the uncertainty state vector $\underline{q}(t)$ is given by (see Fig. 5)

$$\underline{q}(t) = \begin{bmatrix} q_{p1}^1 & q_{p1}^2 & q_{p2}^1 & q_{p2}^2 & q_{s1} & q_{s2} \end{bmatrix}^T \tag{40}$$

and D is a constant matrix given by

$$D = \begin{bmatrix} 0^{(1\times 8)} & 0 & 0 & 0 & 0 & 0 & 0 & 0 & 0 & 0 \\ 0^{(1\times 8)} & \beta_{p1} & 0 & 0 & 0 & 0 & 0 & 0 & 0 & 0 \\ 0^{(1\times 8)} & 0 & 0 & 0 & 0 & 0 & 0 & 0 & 0 & 0 \\ 0^{(1\times 8)} & 0 & 0 & \beta_{p2} & 0 & 0 & 0 & 0 & 0 & 0 \\ 0^{(1\times 8)} & 0 & 0 & 0 & 0 & \beta_{s1} & 0 & 0 & 0 & 0 \\ 0^{(1\times 8)} & 0 & 0 & 0 & 0 & 0 & 0 & \beta_{s2} & 0 & 0 \end{bmatrix}^T \tag{41}$$

Thus, we can put the system in the feedback form shown in Fig. 8, where system H_1 is given by Eq. (39)

$$\dot{\underline{e}} = m(\underline{e},\underline{q}) = G\underline{e}(t) + f_1(\underline{e}(t)) - D\underline{q}(t)$$

$$y_1 = \begin{bmatrix} V_{p1} & V_{p2} & V_{s1} & V_{s2} \end{bmatrix}^T \tag{42}$$

and system H_2 includes the uncertainty dynamics of all four actuators (Eqs. (9))

$$\dot{\underline{q}} = G_q\underline{q} + D_q y_1$$

$$y_2 = \underline{q} \tag{43}$$

where G_q and D_q are given by

$$G_q = \begin{bmatrix} 0 & 1 & 0 & 0 & 0 & 0 \\ -m_{p1}^2 & -2m_{p1} & 0 & 0 & 0 & 0 \\ 0 & 0 & 0 & 1 & 0 & 0 \\ 0 & 0 & -m_{p2}^2 & -2m_{p2} & 0 & 0 \\ 0 & 0 & 0 & 0 & -m_{s1} & 0 \\ 0 & 0 & 0 & 0 & 0 & -m_{s2} \end{bmatrix} \tag{44}$$

$$D_q = \begin{bmatrix} 0 & 0 & 0 & 0 \\ \delta_{p1} & 0 & 0 & 0 \\ 0 & 0 & 0 & 0 \\ 0 & \delta_{p2} & 0 & 0 \\ 0 & 0 & \delta_{s1} & 0 \\ 0 & 0 & 0 & \delta_{s2} \end{bmatrix} \tag{45}$$

If we can now show that both systems, $H_i: \mathcal{L}_e^4 \rightarrow \mathcal{L}_e^4$, are small-signal finite-gain $\mathcal{L}_\infty$ stable

$$\|y_{i\tau}\|_{L_\infty} \leq \gamma_i \|e_{i\tau}\|_{L_\infty} + \beta_i \quad \forall\, e_i \in \mathcal{L}_e^4$$

with

$$\sup_{0\leq t\leq\tau} \|e_i(t)\| \leq r_i \tag{46}$$

for all $\tau \in [0,\infty)$ (for $i=1,2$), and also show that $\gamma_1\gamma_2 < 1$, then by the small gain theorem [2,14] we can conclude that the feedback connection in Fig. 8 is also small-signal finite-gain L_∞ stable and therefore conclude robustness to actuator multiplicative uncertainties. Note that in Eq. (46), we needed to define mapping H_i in terms of extended spaces $\mathcal{L}_e$ since input $e_i \in \mathcal{L}^4$ may generate an output y_i that does not belong to $\mathcal{L}^4$. Moreover, we look at the truncation of functions up to time τ

$$f_\tau = \begin{cases} f(t) & 0 \leq t \leq \tau \\ 0 & \tau < t \end{cases} \tag{47}$$

In order to show small-signal finite-gain $\mathcal{L}_\infty$ stability of systems H_1 and H_2, we need to use the following theorem, which is presented in Ref. [14].

THEOREM 5.1. *Consider the system*

$$\dot{x} = f(t,x,u) \quad x(0) = x_o$$

$$y = h(t,x,u) \tag{48}$$

Let $B_x = \{x \in \mathbb{R}^n \,|\, \|x\| < r\}$, $B_u = \{u \in \mathbb{R}^m \,|\, \|u\| < r_u\}$, $f: [0,\infty) \times B_x \times B_u \rightarrow \mathbb{R}^n$ be piecewise continuous in t and locally Lipschitz in (x,u), and $h: [0,\infty) \times B_x \times B_u \rightarrow \mathbb{R}^q$ be piecewise continuous in t and continuous in (x,u). Suppose that

(1) $x=0$ is an exponentially stable equilibrium point of $\dot{x} = f(t,x,0)$ and there is a Lyapunov function $v(t,x)$ that satisfies

$$c_1\|x\|^2 \leq v(t,x) \leq c_2\|x\|^2$$

$$\dot{v}(t,x) \leq -c_3\|x\|^2$$

$$\left\| \frac{\partial v}{\partial x} \right\| \leq c_4\|x\| \tag{49}$$

for all $(x,t) \in [0,\infty) \times B_x$ for some positive constants $c_1 - c_4$;

(2) f and h satisfy the inequalities

$$\|f(t,x,u) - f(t,x,0)\| \leq L\|u\| \tag{50}$$

$$\|h(t,x,u)\| \leq \eta_1\|x\| + \eta_2\|u\| \tag{51}$$

for all $(t,x,u) \in [0,\infty) \times B_x \times B_u$ for some nonnegative constants L, η_1, and η_2. Then, for each x_o with $\|x_o\| < r\sqrt{c_1/c_2}$, the system in Eq. (48) is small-signal finite-gain $\mathcal{L}_\infty$ stable. In particular, for each $u \in \mathcal{L}_\infty$ with $\sup_{0\leq t\leq\tau}\|u(t)\| < \min\{r_u, c_1c_3r/c_2c_4L\}$, the output $y(t)$ satisfies

$$\|y_\tau\|_{\mathcal{L}_\infty} \leq \gamma\|u_\tau\|_{\mathcal{L}_\infty} + \beta, \quad \forall\, \tau \in [0,\infty) \tag{52}$$

$$\gamma = \eta_2 + \frac{\eta_1 c_2 c_4 L}{c_1 c_3} \qquad \beta = \eta_1\|x_o\|\sqrt{c_2/c_1} \tag{53}$$

The proof of this theorem can be found in Ref. [14]. For our particular application, in order to show small-signal finite-gain $\mathcal{L}_\infty$ stability of system H_1, let us first notice that in Sec. 5.1 we have shown that $\underline{e}=0$ is an exponential equilibrium point of system $\dot{\underline{e}} = m(\underline{e},0)$. Also, by defining the Lyapunov function $v(\underline{e})$ as in Eq. (32), we obtain the bounds c_1, c_2, and c_4 for $v(\underline{e})$ given by Eqs. (34) and (36), and $\exists r > 0$ such that for all $\|\underline{e}\| < r$, bound c_3 for $\dot{v}(\underline{e})$ is given by Eq. (38). Furthermore, by looking at Eqs. (39) and (50) we can easily obtain the value for L since

$$\|m(\underline{e},\underline{q}) - m(\underline{e},0)\| = \|D\underline{q}\| \leq \sigma_{\max}(D)\|\underline{q}\| \tag{54}$$

Then, after obtaining η_1 and η_2 to satisfy the inequality in Eq. (51), we invoke Theorem 1 to conclude that system H_1 (Eq. (42)) is small-signal finite-gain $\mathcal{L}_\infty$ stable and satisfies Eq. (46) with γ_1 and β_1 given by

$$\gamma_1 = \eta_2 + \frac{\eta_1\sigma_{\max}(D)\lambda_{\max}^2(P)}{\lambda_{\min}(P)\lambda_{\min}(Q)(1-\alpha)}$$

$$\beta_1 = \eta_1\|\underline{e}(0)\|\sqrt{\lambda_{\max}(P)/\lambda_{\min}(P)} \tag{55}$$

with $0 < \alpha < 1$. It is clear that the selection of matrix Q in Eq. (33) directly affects the value of γ_1 in Eq. (55). Thus, in order to obtain a small value for γ_1, let T be composed by the eigenvectors (and generalized eigenvectors) corresponding to the eigenvalues of matrix G, and perform the similarity transformation $\underline{e} = T\underline{\bar{e}}$. The system in Eq. (42) then becomes

$$\frac{d\underline{\bar{e}}}{dt} = T^{-1}GT\underline{\bar{e}} + T^{-1}f_1(T\underline{\bar{e}}) - T^{-1}D\underline{q} = \bar{G}\underline{\bar{e}} + \bar{f}_1(\underline{\bar{e}}) - \bar{D}\underline{q}$$

$$y_1 = \underline{u}(T\underline{\bar{e}}) \tag{56}$$

As with the original realization of system H_1, it can be shown that $\exists r > 0$ such that for all $\|\underline{\bar{e}}\| < r$ the inequality in Eq. (46) is satisfied with γ_1 and β_1 given by

$$\gamma_1 = \eta_2 + \frac{\eta_1\sigma_{\max}(T)\sigma_{\max}(T^{-1}D)\lambda_{\max}^2(\bar{P})}{\lambda_{\min}(\bar{P})\lambda_{\min}(\bar{Q})(1-\alpha)}$$

$$\beta_1 = \eta_1\sigma_{\max}(T)\|T\underline{e}(0)\|\sqrt{\lambda_{\max}(\bar{P})/\lambda_{\min}(\bar{P})} \tag{57}$$

with $0 < \alpha < 1$, where $\bar{P}$ and $\bar{Q}$ satisfy the Lyapunov equation

$$\bar{G}^T\bar{P} + \bar{P}\bar{G} = -\bar{Q} \tag{58}$$

with $\bar{P} = T^TPT$ and $\bar{Q} = T^TQT$. This time, however, since matrix $\bar{G}$ is in Jordan form, we can select matrix $\bar{Q}$ so that the ratio $\lambda_{\max}^2(\bar{P})/\lambda_{\min}(\bar{P})\lambda_{\min}(\bar{Q})$ in γ_1 (Eq. (57)) is small.

We can similarly show that system H_2 (Eq. (43)) is small-signal finite-gain $\mathcal{L}_\infty$ stable and obtain gains γ_2 and β_2. Now, by using the controller gains used to obtain the simulation results shown in Fig. 7, we obtain the values for γ_i and β_i $(i=1,2)$ shown in Table 1. Thus, since $\gamma_1\gamma_2 < 1$, we conclude from the small gain theorem that the feedback connection in Fig. 8 is small-signal finite-gain L_∞ stable, and therefore, the control system is robust to the actuator multiplicative uncertainties in Eq. (9). The results presented in this proof have been used for the uncertainty coefficients defined in Sec. 3; however, similar results can be obtained for $0.5 \leq \delta_{ji} \leq 1.5$ and $1.3 \leq m_{ji} \leq 5$ for $j=p,s$ and $i=1,2$.

5.3 Robustness of the Dynamic Feedback Linearization Control Strategy. For the case of the *Dynamic Feedback Linearization* controller described in Sec. 3, we can perform a similar analysis. First, we obtain the error dynamics

Table 1 Gains required to show small-signal finite-gain $\mathcal{L}_\infty$ stability of systems H_1 and H_2 for the *Robust Feedback Linearization Plus Inner Loops* (RFLPIL) controller and the *Dynamic Feedback Linearization* (DFL) controller

RFLPIL controller	DFL controller
$\gamma_1=3.04$	$\gamma_1=762.04$
$\beta_1=1.05$	$\beta_1=0.36$
$\gamma_2=0.27$	$\gamma_2=0.16$
$\beta_2=0.002$	$\beta_2=0.003$

$$\dot{\tilde{x}}_e = \bar{m}(\tilde{x}_e, q) = f(\tilde{x}_e) - Dq(t) \tag{59}$$

where $\tilde{x}_e$ is the error state vector, $f(\tilde{x}_e)$ is obtained by combining Eqs. (6), (8), and (9), and D and $q(t)$ are defined exactly as in Eq. (39). After linearizing $\dot{\tilde{x}}_e = f(\tilde{x}_e)$ along $\tilde{x}_e = 0$, we can put the system in the form of Fig. 8. We then show the exponential stability of $\tilde{x}_e = 0$ and obtain constants $c_1 - c_4$ as in Eqs. (34), (36), and (38). Once L, η_1, and η_2 are obtained as described in Sec. 5.2, we use Eq. (57) to compute gains γ_1 and β_1. Gains γ_2 and β_2 for system H_2 in Fig. 8 are similarly obtained. Then, using the same controller gains as those used to obtain the results shown in Fig. 4, we calculate the values for γ_i and β_i $(i=1,2)$ shown in Table 1. As seen in this table, this time $\gamma_1\gamma_2 > 1$, and thus, we cannot conclude anything from the small gain theorem; however, such a large value for γ_1 indicates that the system may not be robust to actuator multiplicative uncertainties. Note that not only the same controller gains used in Sec. 3 produced such a large value for γ_1, but we were not able to find any set of controller gains that would satisfy our control objective and at the same time obtain boundaries η_1 and η_2 that would make γ_1 small enough so that $\gamma_1\gamma_2 < 1$.

6 Experimental Results

The conclusions just made regarding the robustness of the two control strategies presented are justified not only by the simulation results shown in Figs. 4 and 7 but also through experimental tests. Figure 9 shows experimental results when a sheet of finite length was introduced to the steerable nips section and we used the *Robust Feedback Linearization Plus Inner Loops* controller described in Sec. 4. Here, the lateral and longitudinal position of the page is defined by the position of the leading right corner of the page (point C in Fig. 1). Figure 9 shows that we were able to correct the sheet's position in about 0.3 s. Note that the longitudinal position increases steadily because the sheet moves in the longitudinal direction at all times. The small discrepancies observed between simulation and experimental results can be attributed to sensor noise and unmodeled dynamics.

When the *Dynamic Feedback Linearization* controller presented in Sec. 3 was tested on the experimental setup, it went unstable very quickly, and we were not able to collect any data because we did not want to risk the safety of our setup. However, in order to illustrate this instability, we performed a hybrid experiment, in which the real actuators were used, but we simulated the sheet by using the kinematics model. Those results are presented in Fig. 10, showing that this controller is not able to correct for the sheet initial position errors.

7 Conclusion

In this paper we have shown the drawbacks of using a controller simply based on *Dynamic Feedback Linearization* due to unmodeled dynamics. Furthermore, we presented a robust modified version, which we call *Robust Feedback Linearization Plus Inner Loops* controller. Not only did we prove that this control strategy is robust to multiplicative uncertainties, but we also showed its successful implementation. This control strategy separates kinematics from actuator dynamics and uses feedback linearization

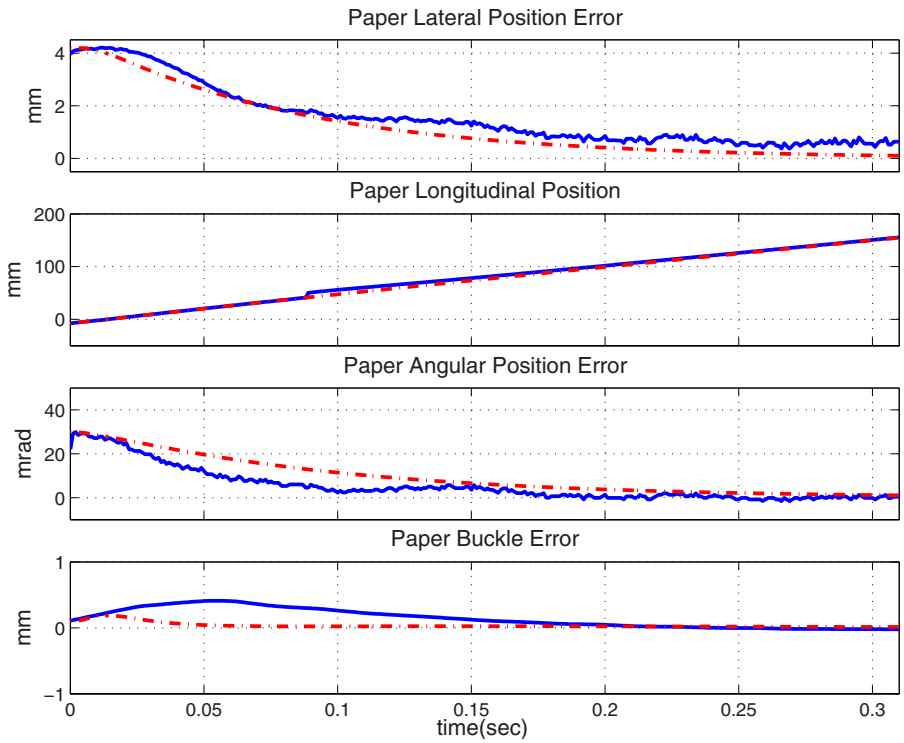

Fig. 9 Experimental results using the *Robust Feedback Linearization Plus Inner Loops* controller. The solid line is used for experimental results and the dashed line is used for simulation results.

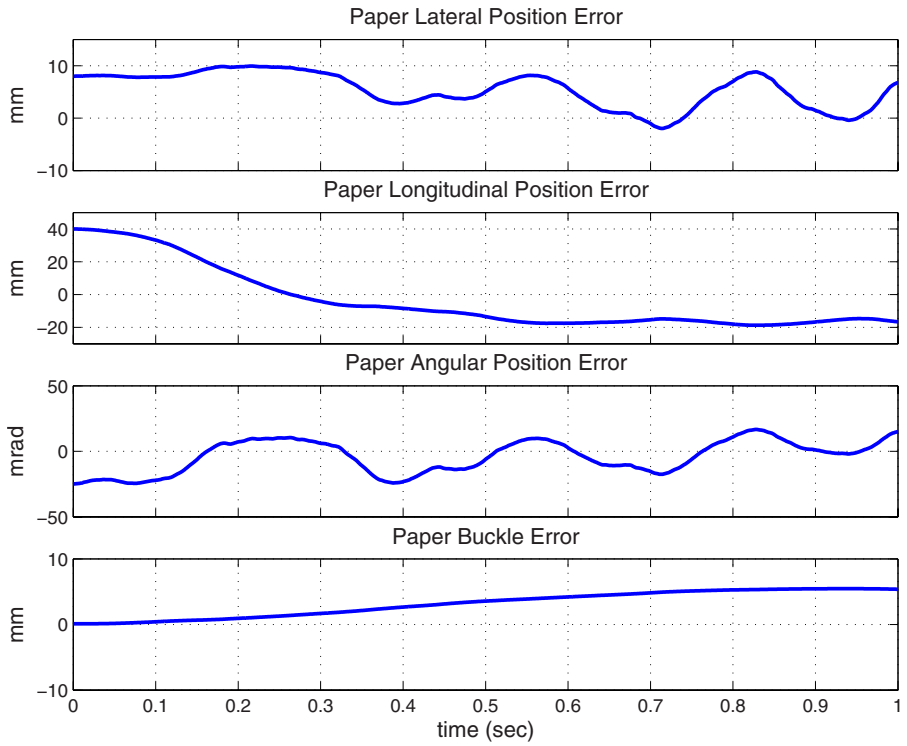

Fig. 10 Hybrid experimental results using the *Dynamic Feedback Linearization* controller, where real actuators were used, but the sheet response was simulated using the kinematic model

only in the kinematics part of the system. Then it uses internal loops to locally control the rotational velocity and steering position of the rollers through standard dynamic linear controllers. Besides simulation and experimental results, we have also presented a formal proof that corroborates our findings.

Acknowledgment

This work was supported by the National Science Foundation under Grant No. CMS 0301719 and by Xerox Corporation.

References

[1] Isidori, A., 1995, *Nonlinear Control Systems*, 3rd ed., Springer, New York.
[2] Shankar Sastry, S., 1999, *Nonlinear Systems: Analysis, Stability, and Control*, Springer, New York.
[3] Descusse, J., and Moog, C. H., 1985, "Decoupling With Dynamic Compensation for Strong Invertible Affine Non-Linear Systems," Int. J. Control, **42**(6), pp. 1287–1398.
[4] d'Andrea-Novel, B., Campion, G., and Bastin, G., 1995, "Control of Nonholonomic Wheeled Mobile Robots by State Feedback Linearization," Int. J. Robot. Res., **14**, pp. 543–559.
[5] Ergueta, E., Sanchez, R., Horowitz, R., and Tomizuka, M., 2010, "Convergence Analysis of a Steerable Nips Mechanism for Full Sheet Control in Printing Devices," ASME J. Dyn. Syst., Meas., Control, **132**(1), p. 011008.
[6] Ergueta, E., Sanchez, R., Horowitz, R., and Tomizuka, M., 2007, "A Mechatronic Approach to Full Sheet Control Using Steer-Able Nips," ASME, Seattle, WA, Nov. 11–15.
[7] Sanchez, R., Horowitz, R., and Tomizuka, M., 2004, "Paper Sheet Control Using Steerable Nips," The American Control Conference Proceedings, pp. 482–487, Boston, MA, Jun. 30–Jul. 2.
[8] Sanchez, R., Ergueta, E., Fine, B., Horowitz, R., Tomizuka, M., 2006, and Krucinskić, M., "A Mechatronic Approach to Full Sheet Control Using Steer-Able Nips," The Fourth IFAC Symposium in Mechatronic Systems, Heidelberg, Germany, Sept. 12–15.
[9] Sanchez, R., 2006, "Nonlinear Control Strategies for a Steerable Nips Mechanism," Ph.D. thesis, University of California, Berkeley, CA.
[10] Sanchez, R., Horowitz, R., and Tomizuka, M., 2010, "Full Sheet Control Using Steerable Nips," IEEE/ASME Trans. Mechatron., **15**(1), pp. 48–58.
[11] Hwang, S. S., 2002, "Sheet Registration and Deskewing System With Independent Drives and Steering," U.S. Patent No. 6,634,521.
[12] Yun, X., and Sarkar, N., 1996, "Dynamic Feedback Control of Vehicles With Two Steerable Wheels," The IEEE International Conference on Robotics and Automation, pp. 3105–3110.
[13] Swaroop, D., Gerdes, J. C., Yip, P. P., and Hedrick, J. K., 1997, "Dynamic Surface Control of Nonlinear Systems," Proceedings of the American Control Conference, Albuquerque, NM, pp. 3028–3034.
[14] Khalil, H. K., 1996, *Nonlinear Systems*, 2nd ed., Prentice Hall, Englewood Cliffs, NJ.